Munc18-1 is a molecular chaperone for α-synuclein, controlling its self-replicating aggregation

Ye Jin Chai,[1]* Emma Sierecki,[2,3]* Vanesa M. Tomatis,[1] Rachel S. Gormal,[1] Nichole Giles,[2,3] Isabel C. Morrow,[1] Di Xia,[1] Jürgen Götz,[1] Robert G. Parton,[2] Brett M. Collins,[2] Yann Gambin,[2,3] and Frédéric A. Meunier[1]

[1]Clem Jones Centre for Ageing Dementia Research, Queensland Brain Institute and [2]Institute for Molecular Bioscience, The University of Queensland, Brisbane, Queensland 4072, Australia
[3]Single Molecule Sciences Centre, European Molecular Biology Laboratory Australia, The University of New South Wales, Sydney 2052, Australia

Munc18-1 is a key component of the exocytic machinery that controls neurotransmitter release. Munc18-1 heterozygous mutations cause developmental defects and epileptic phenotypes, including infantile epileptic encephalopathy (EIEE), suggestive of a gain of pathological function. Here, we used single-molecule analysis, gene-edited cells, and neurons to demonstrate that Munc18-1 EIEE-causing mutants form large polymers that coaggregate wild-type Munc18-1 in vitro and in cells. Surprisingly, Munc18-1 EIEE mutants also form Lewy body–like structures that contain α-synuclein (α-Syn). We reveal that Munc18-1 binds α-Syn, and its EIEE mutants coaggregate α-Syn. Likewise, removal of endogenous Munc18-1 increases the aggregative propensity of α-Syn^{WT} and that of the Parkinson's disease–causing α-Syn^{A30P} mutant, an effect rescued by Munc18-1^{WT} expression, indicative of chaperone activity. Coexpression of the α-Syn^{A30P} mutant with Munc18-1 reduced the number of α-Syn^{A30P} aggregates. Munc18-1 mutations and haploinsufficiency may therefore trigger a pathogenic gain of function through both the corruption of native Munc18-1 and a perturbed chaperone activity for α-Syn leading to aggregation-induced neurodegeneration.

Introduction

Munc18-1 is an essential component of the molecular machinery that controls SNARE-mediated membrane fusion in neurons and neuroendocrine cells. It acts by transporting a SNARE protein called syntaxin1A to the plasma membrane (Han et al., 2009; Malintan et al., 2009; Martin et al., 2013; Papadopulos et al., 2013) and by regulating the formation of the SNARE complex during synaptic vesicle priming, a process that drives the fusion of synaptic vesicles, thereby mediating neurotransmitter release at the synapse. A milestone study demonstrated that Munc18-1 knockout leads to perinatal paralysis-induced lethality but, importantly, does not affect brain development (Verhage et al., 2000). Recently, however, Munc18-1 heterozygous mutations have been associated with several developmental diseases, including nonsyndromic intellectual disability, epilepsy (Hamdan et al., 2009, 2011; Deprez et al., 2010; Otsuka et al., 2010; Mignot et al., 2011), and early infantile epileptic encephalopathy (EIEE; Saitsu et al., 2008, 2010). EIEEs comprise a group of rare but severe developmental disorders, with a poor initial prognosis (50% of patients die within the first year; Tavyev Asher and Scaglia, 2012; Barcia et al., 2014). Munc18-1 mutations linked to the development of EIEE4 include intragenic and whole-gene deletions, as well as 10 different missense mutations (Saitsu et al., 2008, 2010; Otsuka et al., 2010). The mechanism by which these mutations lead to the pathological epileptic phenotype is poorly understood and may involve either haploinsufficiency of the wild-type (WT) protein or a gain of pathological function of the mutant allele. In addition, dysregulation of Munc18-1 expression has been associated with other neurological disorders, including Alzheimer's disease (Jacobs et al., 2006; Donovan et al., 2012) and Rasmussen encephalitis (Alvarez-Barón et al., 2008). In this study, we reveal a critical new role for Munc18-1 in chaperoning α-synuclein (α-Syn), thereby controlling its aggregative propensity and ability to form toxic α-Syn oligomers.

Results

The Munc18-1^{C180Y} mutation induces coaggregation of Munc18-1^{WT} in a cell-free system

In a recent study, we demonstrated that expression of Munc18-1 carrying the missense EIEE4-causing mutation (C180Y; Fig. 1 A) leads to its cellular aggregation, with catastrophic

*Y.J. Chai and E. Sierecki contributed equally to this paper.

Correspondence to Frederic A. Meunier: f.meunier@uq.edu.au; or Yann Gambin: y.gambin@unsw.edu.au

Abbreviations used: ANOVA, analysis of variance; CRISPR/Cas9, clustered regularly interspaced short palindromic repeats/Cas9; EIEE, epileptic infantile epileptic encephalopathy; MKO, Munc18-1 knockout; PAM, protospacer adjacent motif; PD, Parkinson's disease; sgRNA, single guide RNA; WT, wild type.

The Rockefeller University Press $30.00
J. Cell Biol. Vol. 214 No. 6 705–718
www.jcb.org/cgi/doi/10.1083/jcb.201512016

effects on neuroexocytosis (Martin et al., 2014). The mutation promotes misfolding and aggregation, potentiating the protein's ubiquitination and degradation by the proteasome, thereby inhibiting its availability for membrane fusion (Saitsu et al., 2008; Martin et al., 2014). We also examined the process of Munc18-1^{C180Y} aggregation using single-molecule fluorescence spectroscopy to directly assess oligomerization of fluorescently tagged Munc18-1^{WT} and Munc18-1^{C180Y} expressed in a eukaryotic-cell-free system (Martin et al., 2014). These experiments revealed the existence of large aggregates of Munc18-1^{C180Y}, as indicated by the detection of bright particles, detected as large fluctuations in fluorescence intensity that were never observed for Munc18-1^{WT} molecules (Martin et al., 2014). As widespread aggregation was observed in Munc18-1^{C180Y}-expressing cells, we questioned whether these could contribute to a dominant pathological function by incorporating the WT Munc18-1 protein. We first performed two-color coexpression experiments and examined the ability of the Munc18-1^{C180Y} mutant to incorporate Munc18-1^{WT} proteins into large aggregates by two-color single-molecule detection (Martin et al., 2014; Fig. 1, B–E). We observed that the C180Y mutant and WT proteins indeed coaggregated (Fig. 1 D). Coincidental detection of the two labels was widespread (Fig. 1 E), confirming the incorporation of Munc18-1^{WT} in most Munc18-1^{C180Y} aggregates.

Importantly, in coexpression experiments in vitro, we did not observe a random aggregation process (identified by frequent fluorescence bursts with widely varying size distributions) but rather detected relatively rare and very large bursts of fluorescence intensity (Fig. 1 D). This suggested an ordered self-association and the formation of polymer-like structures that extend by recruitment of monomers. In this scenario, once a small aggregate is formed, this "seed" can recruit new proteins and elongate/grow to form larger fibrils. To test the potential formation of self-propagating aggregates, we performed two-color experiments incorporating preformed seeds of aggregated Munc18-1^{C180Y} (Fig. 1, F–H). Munc18-1^{C180Y} tagged with mCherry was first expressed separately, purified by centrifugation and fragmented by sonication (Fig. 1 F). These "seeds" were added to a solution of purely monomeric Munc18-1^{C180Y} tagged with GFP. Within a few minutes, we detected the polymerization of Munc18-1^{C180Y}-GFP triggered by the Munc18-1^{C180Y}-mCherry "seeds," indicating self-replication properties. Most interestingly, we also detected a similar recruitment of Munc18-1^{WT} monomers to Munc18-1^{C180Y} seeds (Fig. 1 G), suggesting that Munc18-1^{C180Y} can convert Munc18-1^{WT} into an aggregative form. Coincidental detection of the two labels also confirmed incorporation of Munc18-1^{WT} in most Munc18-1^{C180Y} aggregates (see Fig. 1 H for individual bursts and Fig. 1 I for quantification of recruitment of the Munc18-1^{WT} on the Munc18-1^{C180Y} seeds).

Munc18-1 EIEE4-causing mutations coaggregate Munc18-1^{WT} and form Lewy body–like structures

We next examined Munc18-1 aggregative behavior in cells. We first engineered gene-edited PC12 cells lacking Munc18-1 using the clustered regularly interspaced short palindromic repeats/Cas9 (CRISPR-Cas9) system (Fig. 2 A and Fig. S1 A) in order to perform dual-expression experiments mimicking the heterozygous nature of EIEE4 disorders. Western blotting of Munc18-1 knockout (MKO) PC12 cells revealed no expression of endogenous Munc18-1 (Fig. 2 B). Furthermore, neuroexocytosis in these cells was significantly compromised, and this was restored to normal levels by Munc18-1^{WT} overexpression (Malintan et al., 2009; Fig. S1, B and C). We also checked the level of overexpression, which was slightly higher than that of endogenous Munc18-1 in PC12 cells (Fig. S1 D). After coexpression of Munc18-1^{WT}-emGFP and Munc18-1^{WT}-mCherry, no fluorescent aggregates could be detected in either the green or the red channel (Fig. 2 C). As expected, large coaggregates could be detected upon coexpression of Munc18-1^{C180Y}-emGFP and Munc18-1^{C180Y}-mCherry. Most interestingly, similar coaggregates were observed in MKO-PC12 cells coexpressing Munc18-1^{WT}-emGFP and Munc18-1^{C180Y}-mCherry (Fig. 2, D and E). Switching tags led to the same coaggregative phenotype (Fig. S2 A), and an identical outcome was observed in PC12 cells (Fig. S2, B and C) and rat hippocampal neurons (Fig. 2, F–H; and Fig. S2 A). Importantly, we tested three other EIEE4-causing mutations selected from each of the known domains of Munc18-1 (Fig. 3, A and B) and found that they also possessed the ability to aggregate Munc18-1^{WT} (Fig. 3, C and D).

Our results (Figs. 2 and 3) demonstrate that EIEE4-causing Munc18-1 mutations trigger the coaggregation of Munc18-1^{WT} in neurons and neurosecretory cells. This raises the possibility that the aggregation could deplete the pool of functional Munc18-1^{WT} in vivo or have additional pathological functions such as those seen in Lewy body dementia (Spillantini et al., 1997; Galvin et al., 1999; Maries et al., 2003) that could contribute to the pathological phenotype of EIEE. In support of this view, we occasionally noticed the formation of structures that were morphologically reminiscent of Lewy bodies in MKO-PC12 cells expressing Munc18-1^{C180Y}-emGFP (Fig. S3 A) or coexpressing Munc18-1^{C180Y}-emGFP and Munc18-1^{WT}-mCherry (Fig. S3 B).

The Munc18-1^{C180Y} mutation induces the coaggregation of α-Syn in a cell-free system

As α-Syn is a key component of Lewy bodies (Polymeropoulos et al., 1997; Burré et al., 2014), we hypothesized that EIEE4-causing Munc18-1 mutations could promote coaggregation of other proteins prone to aggregation such as α-Syn. We therefore investigated whether Munc18-1^{C180Y} was capable of aggregating α-Syn or other proteins involved in neuronal trafficking, such as SNAP25 (Polymeropoulos et al., 1997; Burré et al., 2014). As a control, SOD1, a protein linked to familial amyotrophic lateral sclerosis, was included in the coaggregation analysis. Recent studies have shown that SOD1 has an aggregative behavior (Wang et al., 2009; Lang et al., 2015). Upon coexpression of Munc18-1^{C180Y}-GFP with α-Syn-mCherry in vitro, we found that α-Syn was indeed incorporated into Munc18-1^{C180Y} oligomers (Fig. 4, A and B). This effect was specific as neither SNAP25 (Fig. 4, C and D) nor SOD1 (Fig. 4, E and F) showed similar coaggregation behavior.

Munc18-1^{C180Y} mutation induces the aggregation of α-Syn and the formation of Lewy body–like structures

We next investigated whether Munc18-1^{C180Y} was also capable of promoting α-Syn aggregation in PC12 cells and neurons. Upon coexpression of Munc18-1^{WT}-emGFP and α-Syn-mCherry in PC12 cells, no fluorescent aggregates were detected in either the green or red channel (Fig. 5 A). However, coexpression of Munc18-1^{C180Y}-emGFP and α-Syn-mCherry generated many aggregates nearly all of which were α-Syn

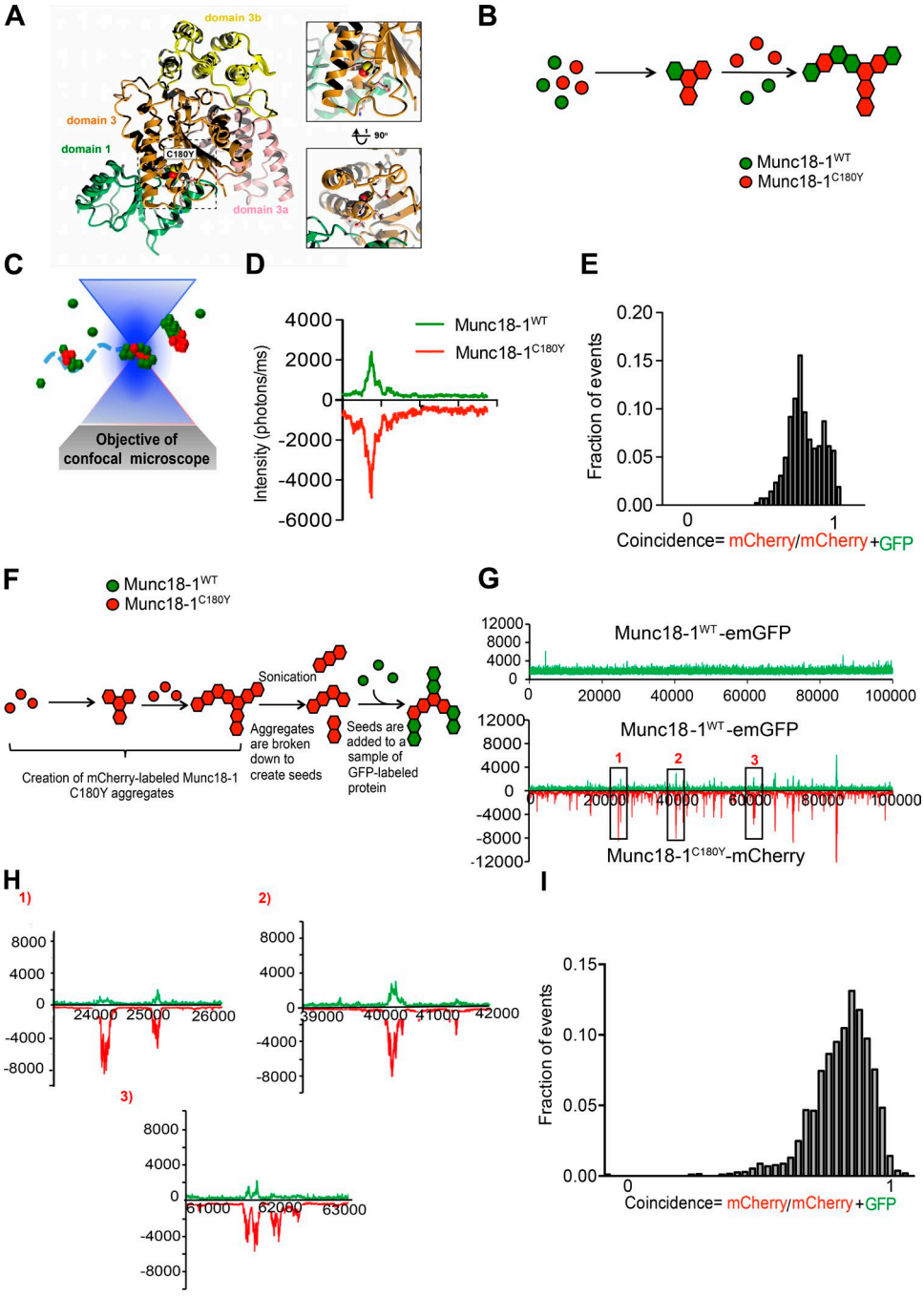

Figure 1. **Munc18-1^{C180Y} induces the coaggregation of Munc18-1^{WT} in vitro.** (A) Structural representation of Munc18-1^{C180Y}. (B) Principle of the coexpression assay. Munc18-1^{C180Y} tagged with mCherry is coexpressed with a GFP-tagged Munc18-1^{WT}. (C) Schematic representation of single-molecule fluorescence experiment in which the proteins freely diffuse in and out of the focal volume created by two lasers simultaneously exciting the GFP and mCherry fluorophores. (D) A single-molecule trace obtained for lysates coexpressing Munc18-1^{WT}-emGFP and Munc18-1^{C180Y}-mCherry. The number of photons detected in the green and red channels are plotted as a function of time. The trace shows a simultaneous burst in both the GFP and mCherry channels that reflects the formation of complexes containing both fluorophores. (E) Histogram of single-molecule coincidence between Munc18-1^{WT}-emGFP and Munc18-1^{C180Y}-mCherry coexpressed in a cell-free system. The coincidence is calculated as the ratio of intensity in the mCherry channel divided by the sum of signals in the GFP and mCherry channels. GFP-only bursts show a coincidence at 0, and mCherry-only oligomers are located at coincidence equal to 1. For the oligomers containing both fluorophores, the coincidence ratio is a measure of the stoichiometry of the assembly. More than 50 individual aggregates were analyzed for the histogram, for a total of 2,600 time points above threshold. (F) Principle of a seeding experiment. Munc18-1^{C180Y}-mCherry is expressed in the *L. tarentolae* extracts, and fibrils are formed. After expression, the sample is spun down, and the aggregates are collected and sonicated to give smaller seeds visible in the mCherry channel. Those seeds are mixed into a solution of Munc18-1^{WT}-emGFP. (G) A single-molecule trace obtained from seeding experiments. Munc18-1^{WT}-GFP is recruited to the seeds of Munc18-1^{C180Y}-mCherry (H) Details of individual bursts representing different aggregates diffusing through the focal volume, clearly showing codiffusion of the two fluorophores. (I) Histogram of single-molecule coincidence between Munc18-1^{WT}-GFP and seeds of Munc18-1^{C180Y}-mCherry. The recruitment of GFP onto the mCherry-labeled seeds was calculated from 88 individual aggregates, representing 3,789 time points.

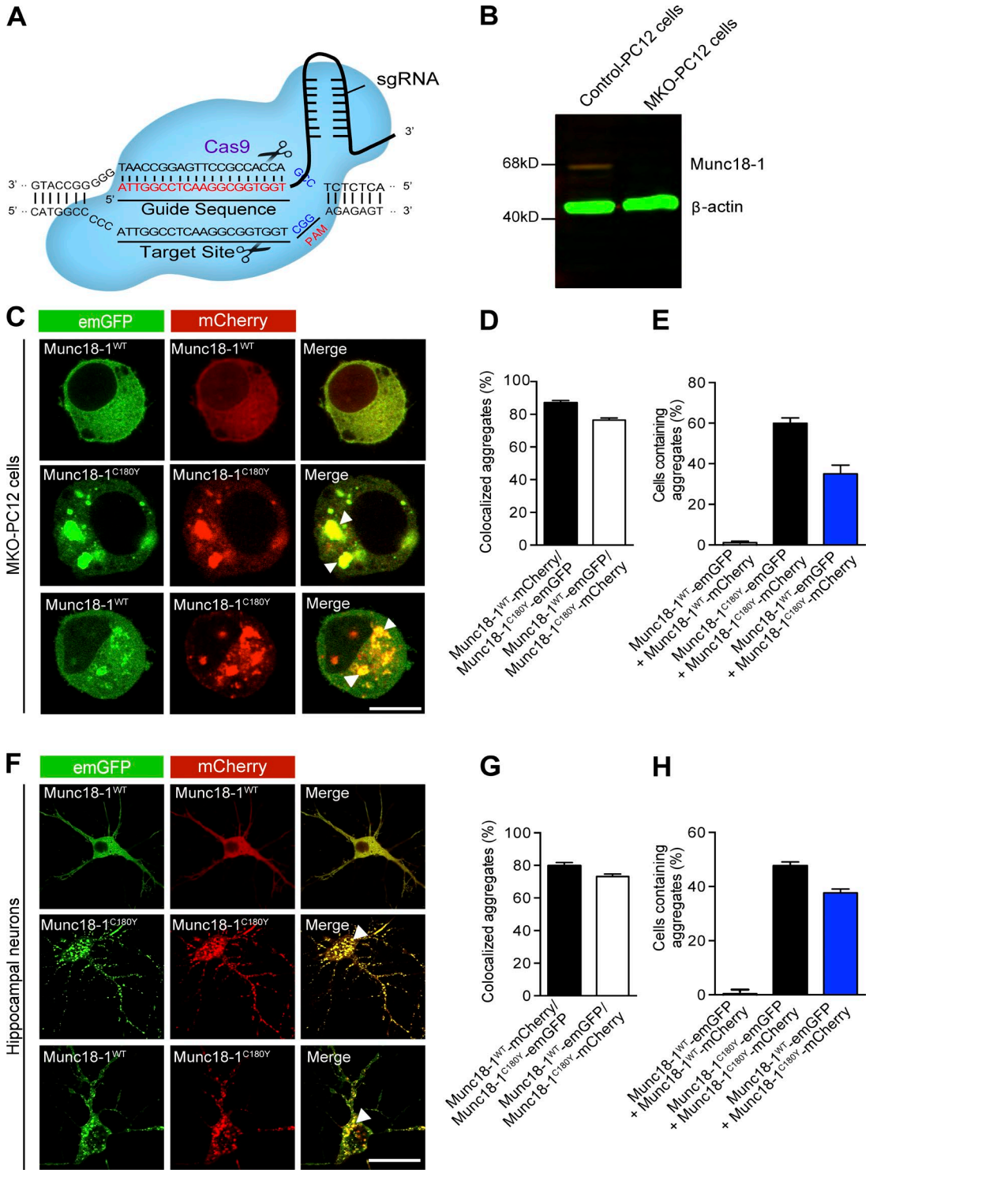

Figure 2. **Munc18-1^{C180Y} mutation coaggregates Munc18-1^{WT} in Munc18-1 knockout PC12 cells and hippocampal neurons.** (A) Schematic diagram of the sgRNA target site. The 20-nt guide sequence comprising the 5′-end of the chimeric single guide RNA (sgRNA) is shown. This sequence pairs with the DNA target site (indicated on the bottom strand). Immediately 3′ to the target sequence is the trinucleotide protospacer adjacent motif (PAM; 5′-NGG). The CAS9 enzyme mediates a double-stranded break (DSB) ∼3 bp upstream of the PAM. (B) Cell lysates of WT (PC12 cells) and clonal Munc18-1 knockout isolates (MKO-PC12 cells) were subjected to Western blot analysis and probed with anti–Munc18-1 (red). A parallel set of lysates was probed with anti–actin antibody as a loading control (green). (C) Representative images showing coaggregates positive for Munc18-1^{C180Y} and Munc18-1^{WT} in MKO-PC12 cells. MKO-PC12 cells were cotransfected with Munc18-1^{WT}-emGFP and Munc18-1^{WT}-mCherry (top), Munc18-1^{C180Y}-emGFP and Munc18-1^{C180Y}-mCherry (middle), or Munc18-1^{WT}-emGFP and Munc18-1^{C180Y}-mCherry (bottom). Bar, 20 µm. Arrowheads indicate colocalized aggregates. (D and E) Percentage of colocalized aggregates per cell and percentage of MKO-PC12 cells containing aggregates. Data represent mean ± SEM; 10–20 cells were analyzed for each independent experiment (n = 7). (F) Representative images showing coaggregates positive for Munc18-1^{C180Y} and Munc18-1^{WT} in hippocampal neurons. Hippocampal neurons (8 d in vitro) were transiently cotransfected with Munc18-1^{WT}-emGFP and Munc18-1^{WT}-mCherry or Munc18-1^{C180Y}-emGFP and Munc18-1^{C180Y}-mCherry or Munc18-1^{WT}-emGFP and Munc18-1 ^{C180Y}-mCherry. Bar, 20 µm. Percentage of colocalized aggregates per neuron (G) and percentage of hippocampal neurons containing aggregates (H). Data represent mean ± SEM; 10–20 neurons were analyzed for each independent experiment (n = 6). Arrowheads indicate the colocalized aggregates.

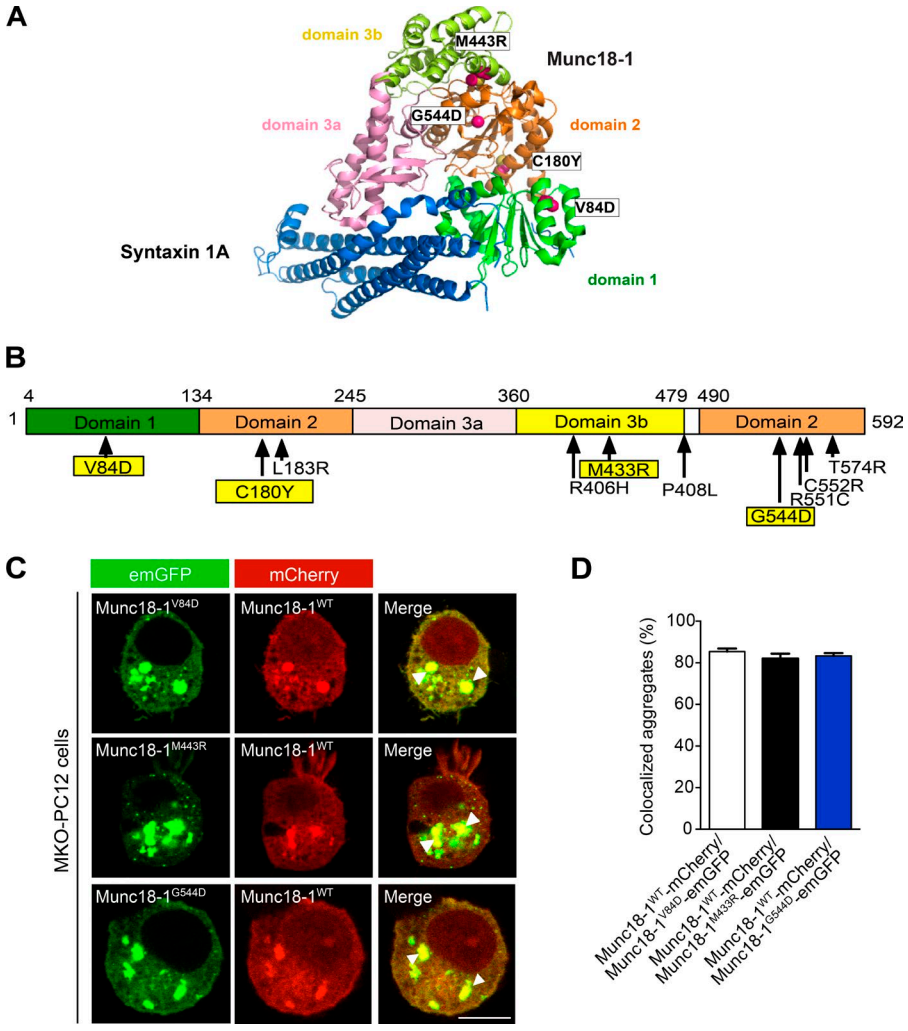

Figure 3. **Munc18-1 EIEE4-causing mutations coaggregate Munc18-1^{WT} in MKO-PC12 cells.** (A) Positions of missense mutations (V84D, M443R, and G544D) in the Munc18-1 crystal structure are shown as a stereo representation. (B) Schematic domain diagram of EIEE4-causing Munc18-1 mutations. (C) Representative images showing coaggregates positive for Munc18-1^{V84D}-emGFP and Munc18-1^{WT}-mCherry (top), Munc18-1^{M443R}-emGFP and Munc18-1^{WT}-mCherry (middle), or Munc18-1^{G544D}-emGFP and Munc18-1^{WT}-mCherry (bottom) are shown. Bar, 20 µm. (D) Percentage of colocalized aggregates per cell. Data represent mean ± SEM; 15–20 cells in each independent experiment were measured; *n* = 5. Arrowheads indicate the colocalized aggregates.

positive (Fig. 5 A). More than 80% of the Munc18-1^{C180Y}–positive aggregates colocalized with α-Syn (Fig. 5 B), and the area occupied by α-Syn–positive aggregates was significantly increased upon Munc18-1^{C180Y}-emGFP coexpression (Fig. 5 C). We also observed the presence of Lewy body–like structures upon expression of Munc18-1^{C180Y}-emGFP and α-Syn-mCherry in MKO-PC12 cells (Fig. S3 C), and similar coaggregation was observed in hippocampal neurons (Fig. 5, D–F).

The specific recruitment of α-Syn to Munc18-1 mutant aggregates suggested that the proteins may also interact under nonpathological situations. We tested this using a pull-down strategy in PC12 cells expressing either Munc18-1^{C180Y}-emGFP or Munc18-1^{WT}-emGFP with α-Syn-mCherry. Both Munc18-1^{WT} and Munc18-1^{C180Y} were immunoprecipitated to the same extent as the GFP-trap beads (Fig. 5 G). Under these conditions, we observed an interaction between Munc18-1^{WT} and α-Syn, although we found that Munc18-1^{C180Y} was able to pull down threefold more α-Syn than Munc18-1^{WT} (Fig. 5 H). This suggests that the native Munc18-1 and α-Syn proteins are able to interact with each other but that the aggregation of the Munc18-1^{C180Y} mutant then sequesters more α-Syn as it oligomerizes. Importantly, expression of Munc18-1^{C180Y}-emGFP, as well as several other EIEE4-linked Munc18-1 mutants, also recruited endogenous α-Syn to these structures (Figs. 6, A–C). Similarly, expression of Munc18-1^{C180Y}-emGFP in hippocampal neurons led to the aggregation of endogenous α-Syn and the formation of Lewy body–like structures (Fig. 7, A and B). We used correlative fluorescence electron microscopy to further investigate the ultrastructure of these large aggregates in MKO-PC12 cells and found relatively disorganized electron-dense protein aggregates (Fig. 7 C). More interestingly, we noted that the expression of Munc18-1^{C180Y}-emGFP in hippocampal neuron produced a much higher proportion of pyknotic nuclei compared with neurons expressing Munc18-1^{WT}-emGFP, demonstrating that these cells were indeed undergoing or about to undergo cell death (Fig. 7, D and E). Moreover, neurites from these Munc18-1^{C180Y}-emGFP–expressing neurons exhibited classical signs of neurodegeneration, including the presence of spheroids (Fig. 7 D) that are inherent to degenerative neurons conditions such as Alzheimer's disease (Orimo et al., 2008). Munc18-1^{C180Y}-emGFP is therefore sufficient to confer a neurodegenerative phenotype leading to neuronal cell death (Fig. 7, D and E).

Parkinson's disease–linked α-Syn mutants coaggregate Munc18-1^{WT} and endogenous Munc18-1

These experiments raised the question of whether the reverse scenario was possible: Would expression of a human mutation of α-Syn linked to Parkinson's disease (PD) also lead to coaggregation of Munc18-1^{WT}? Coexpression of either α-Syn^{A53T}-GFP or α-Syn^{A30P}-GFP aggregation-prone mutants with Munc18-1^{WT}-mCherry in MKO-PC12 cells induced a clear aggregation

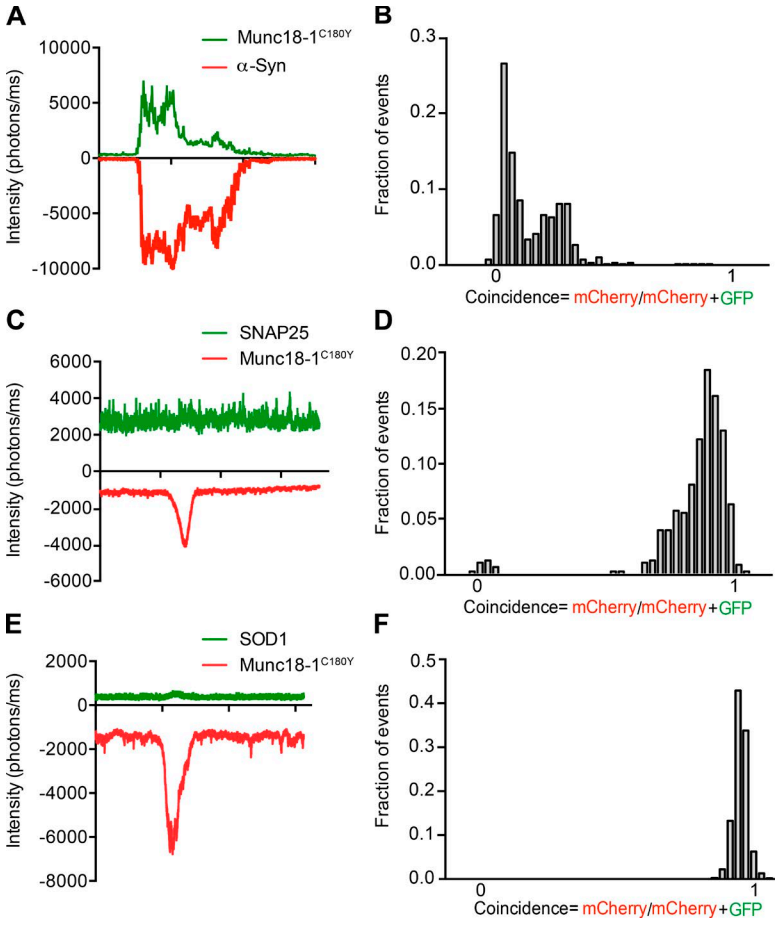

Figure 4. **Single-molecule coincidence mapping of interactions between Munc18-1^{C180Y} and α-Syn.** (A) A single-molecule trace obtained for cell-free lysates coexpressing α-Syn^{WT}-mCherry and Munc18-1^{C180Y}-GFP. The number of photons detected in the green and red channels are plotted as a function of time. The trace shows simultaneous bursts in the GFP and mCherry channels that reflect the formation of complexes containing both fluorophores. (B) Histogram of single-molecule coincidence between α-Syn^{WT}-mCherry and Munc18-1^{C180Y}-GFP coexpressed in a cell-free system. Note that the Munc18-1^{C180Y} aggregates are now located on the left off the histograms, and insertion of the α-Syn^{WT} pushes the distribution to higher stoichiometry values. (C) A single-molecule trace obtained for a cell-free lysate coexpressing SNAP-25-GFP and Munc18-1^{C180Y}-mCherry. The trace shows no simultaneous burst in the GFP and mCherry channels, suggesting that SNAP-25 does not coaggregate with Munc18-1^{C180Y} (D) Histogram of single-molecule coincidence between SNAP-25-GFP and Munc18-1^{C180Y}-mCherry. The diagram indicates that most mCherry-only oligomers are located at coincidence equal to 1. (E) Single-molecule coincidence between SOD1-GFP and Munc18-1^{C180Y}-mCherry coexpressed in a cell-free lysate. (F) Histogram of single-molecule coincidence between SOD1-GFP and Munc18-1^{C180Y}-mCherry. The trace shows that there is no coaggregation between SOD1-GFP and Munc18-1^{C180Y}-mCherry. The data were analyzed based on >40 individual aggregates for each protein pair, representing >2,500 time points.

of Munc18-1^{WT}-mCherry that colocalized with α-Syn mutant GFP-positive structures (Fig. 8, A–C). We also observed Lewy body–like structures in these cells (Fig. S4 A). Importantly, expression of either α-Syn^{A53T}-GFP or α-Syn^{A30P}-GFP was able to recruit endogenous Munc18-1 (Fig. 8, D–F) to form Lewy body–like structures in PC12 cells (Fig. S4 B). We also performed coimmunoprecipitation from solubilized cortical neurons and found that endogenous Munc18-1 strongly interacted with endogenous α-Syn (Fig. S5 A). Moreover, when Munc18-1^{WT}-emGFP and Munc18-1^{C180Y}-emGFP were expressed in PC12 cells, we could detect the interaction of Munc18-1 and endogenous α-Syn (Fig. S5 B).

Munc18-1^{C180Y}-emGFP oligomers in vitro can seed the oligomerization of Munc18-1^{WT}-mCherry (Fig. 1, F–H), suggestive aggregative properties. However, the same seeds were not able to induce the incorporation of α-Syn in vitro (Fig. 9, A and B); hence, the coaggregation of Munc18-1 and α-Syn in cells is likely driven during coexpression.

Munc18-1 acts as a chaperone for α-Syn and controls its aggregative propensity

Some of the EIEE4 disease-causing genetic alterations include partial or full deletion of Munc18-1 gene, suggesting that haploinsufficiency is sufficient to generate a gain of pathological function. We hypothesized that Munc18-1 acts as a chaperone for α-Syn and that knocking out Munc18-1 should be sufficient to alter the propensity of α-Syn to aggregate. To test our hypothesis, we first examined the ability of Munc18-1 to reduce α-Syn^{A30P} oligomer formation in vitro. In support of the chaperone hypothesis, coexpression of Munc18-1 drastically reduced the propensity of α-Syn mutants to form large polymers in single-molecule fluorescence analysis (Fig. 9, C–E). We next investigated whether the level of Munc18-1 affected the aggregation of endogenous α-Syn in neurosecretory cells by comparing the number of α-Syn aggregates in PC12 cells and MKO-PC12 cells. This analysis revealed that knocking out Munc18-1 significantly increased the number of α-Syn aggregates (Fig. 9 F). Importantly, reexpression of Munc18-1 in MKO-PC12 cells significantly reduced these aggregates in a dose-dependent manner (Fig. 9, F–I).

Finally, we compared the number of aggregates formed in MKO-PC12 cells and PC12 cells expressing α-Syn^{WT} and mutants. We found that the number of α-Syn^{WT} aggregates was significantly higher in MKO-PC12 cells than in PC12 cells (Fig. 10). In addition, MKO-PC12 cells expressing α-Syn mutants (A30P and A53T) also exhibited significantly more aggregates than PC12 cells. Importantly, Munc18-1 reexpression in MKO-PC12 cells was sufficient to rescue the number of α-Syn aggregates back to the level detected in PC12 cells (Fig. 10, A–C). Our results therefore suggest that Munc18-1 plays a key role in chaperoning α-Syn and that Munc18-1 haploinsufficiency is sufficient to promote the aggregative phenotype.

Discussion

In this study, we used independent experimental approaches to show that Munc18-1 mutations leading to EIEE4 have

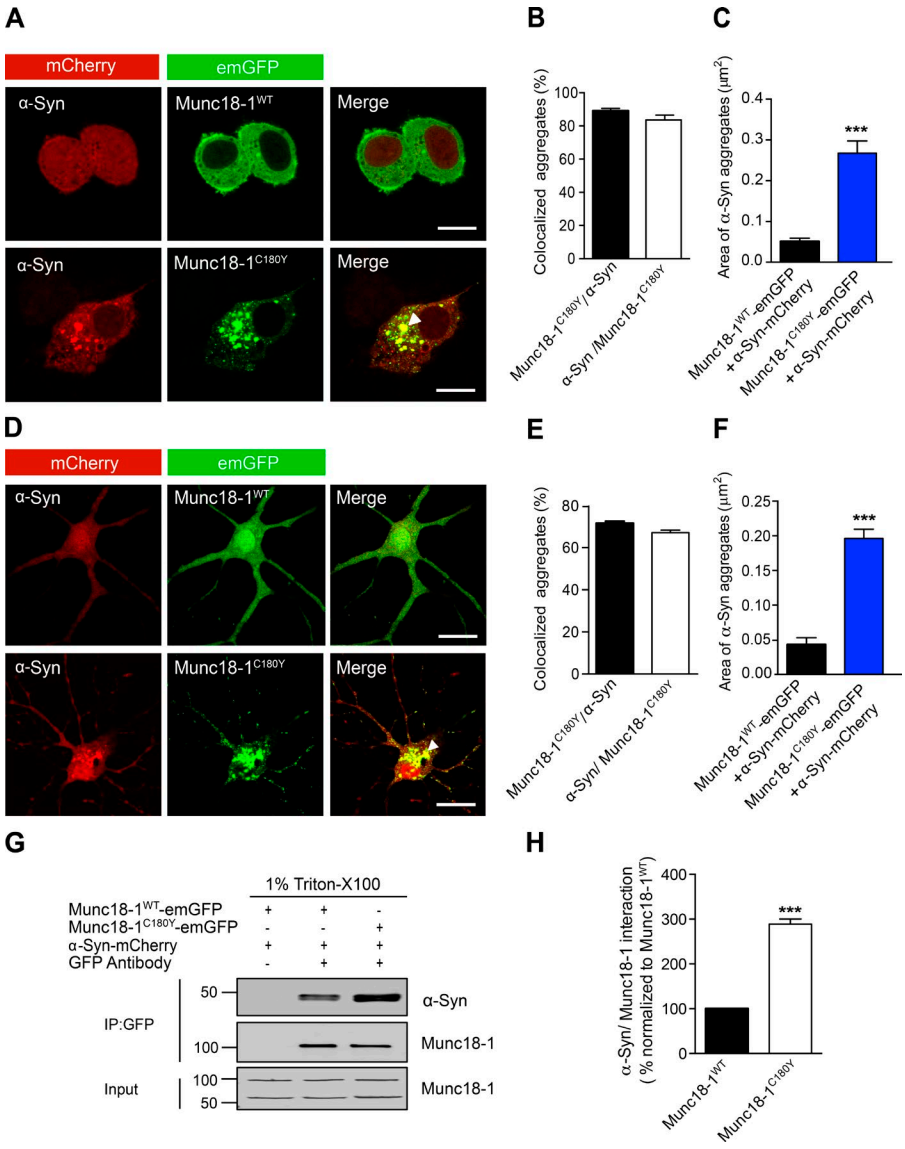

Figure 5. **Munc18-1^{C180Y} mutation induces the aggregation of α-Syn in PC12 cells and hippocampal neurons.** (A) Representative images showing coaggregates positive for α-Syn and Munc18-1^{WT} (top) and α-Syn and Munc18-1^{C180Y} (bottom) in PC12 cells. Bars, 20 µm. Arrowhead indicates the colocalized aggregate. PC12 cells were cotransfected with either α-Syn-mCherry and Munc18-1^{WT}-emGFP or α-Syn-mCherry and Munc18-1^{C180Y}-emGFP. (B) Percentage of colocalized aggregates. (C) Area occupied by α-Syn aggregates. A mean of 8–20 cells were analyzed for each independent experiment (n = 4; ***, $P < 0.001$, unpaired Student's t test). (D) Representative images showing coaggregates positive for α-Syn and Munc18-1^{WT} (top) and α-Syn and Munc18-1^{C180Y} (bottom) in hippocampal neurons. Hippocampal neurons were cotransfected either α-Syn-mCherry and Munc18-1^{WT}-emGFP or α-Syn-mCherry and Munc18-1^{C180Y}-emGFP at 8 d in vitro. Bars, 20 µm. Arrowhead indicates the colocalized aggregates. (E) Percentage of colocalized aggregates. (F) Area occupied by α-Syn aggregates. 10–15 neurons in each independent experiment were analyzed (n = 5; ***, $P < 0.001$, unpaired Student's t test). (G) PC12 cells were either cotransfected with Munc18-1^{WT}-emGFP and α-Syn-mCherry or Munc18-1^{C180Y}-emGFP and α-Syn-mCherry. They were lysed, solubilized, and immunoprecipitated with anti-GFP antibodies. Western blot analysis was performed using anti–α-Syn and anti–Munc18-1 antibodies. (H) The interaction between α-Syn and Munc18-1 was quantified after normalizing against the amount of immunoprecipitated Munc18-1. Data represent mean ± SEM of band intensities normalized to control values of Munc18-1^{WT} (n = 3; ***, $P < 0.001$, unpaired Student's t test).

the ability to coaggregate Munc18-1^{WT} in vitro as well as in neurosecretory cells engineered to knock out Munc18-1 and in hippocampal neurons. The discovery of Lewy body–like structures that were positive for Munc18-1 prompted us to investigate a potential link between Munc18-1 and α-Syn, a hallmark of Lewy bodies in PD (Spillantini et al., 1997; McKeith, 2004). This led us to identify a novel interaction between native Munc18-1 and α-Syn proteins and demonstrate that Munc18-1 EIEE4-linked mutant aggregates incorporate α-Syn. Conversely, two mutants of PD-linked α-Syn also promoted Munc18-1 aggregation, suggesting an underlying overlap between the different neurological diseases that will require further exploration.

Finally, we provide the first evidence that knocking out Munc18-1 is sufficient to promote α-Syn aggregation. Furthermore, reexpression of Munc18-1^{WT} can rescue this phenotype in a dose-dependent manner, suggesting that Munc18-1 haploinsufficiency and mutations lead to an aggregative phenotype. To the best of our knowledge, our study is the first to indicate a functional link between Munc18-1 and α-Syn with clear relevance to pathologies caused by mutations of both molecules.

Munc18-1^{C180Y} leads to α-Syn aggregation

We recently demonstrated that the Munc18-1^{C180Y} human mutation triggers widespread subcellular aggregation (Martin et al., 2014), suggesting that Munc18-1 could also have intracellular aggregative activity. We observed that 30–40% of MKO-PC12 cells expressing the EIEE mutants contain aggregates. This percentage is consistent with our previous findings in PC12 cells. It should be noted, however, that only 20% of N2a cells transfected with the same mutants give rise to large aggregates (Saitsu et al., 2008). We can only assume that these subtle differences stem from the different cell lines used. One possibility is that the level of Munc18-1 mutant expression is lower in N2a cells, thereby reducing its propensity to aggregate. Indeed, the four different mutations lie buried within the hydrophobic core of domains 1, 2, and 3b, making the protein unstable and potentiating its degradation through the proteasome (Martin et al., 2014). Using single-molecule analysis, we first demonstrated that Munc18-1^{C180Y} can self-propagate in vitro. Our results highlight a self-perpetuated aggregation of Munc18-1 mutants, suggesting the existence of a switch between the soluble and aggregated forms of the mutant protein. The ability to template Munc18-1^{WT} aggregation

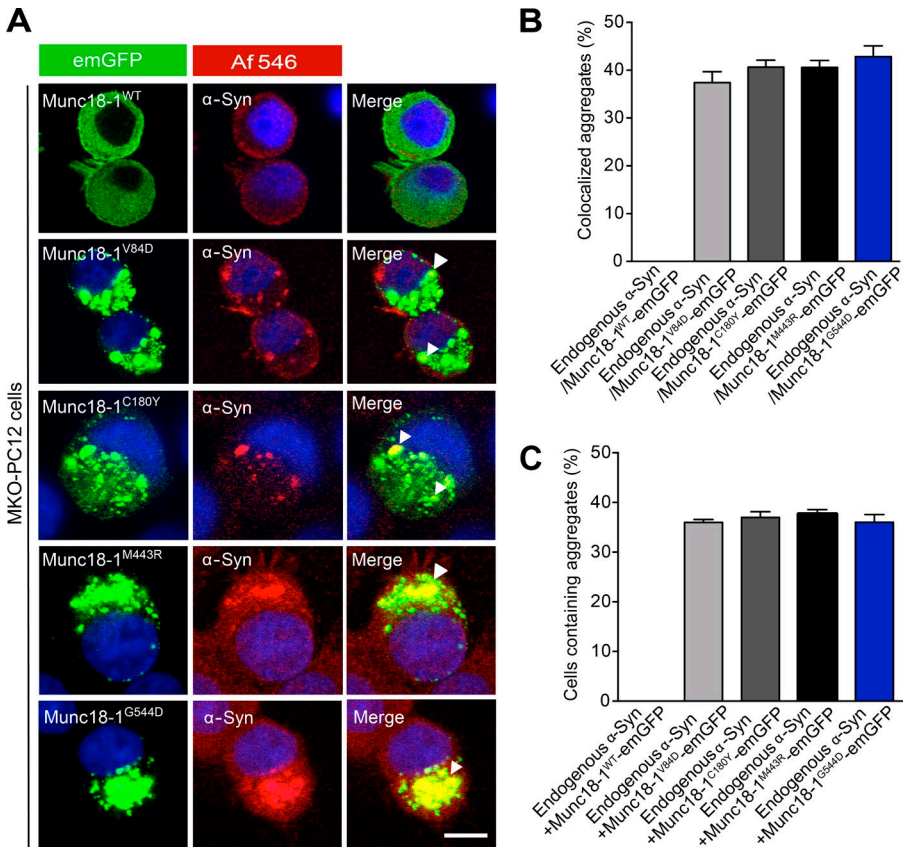

Figure 6. **Munc18-1 EIEE4-causing mutations recruit endogenous α-Syn in MKO-PC12 cells.** (A) MKO-PC12 cells were transfected with EIEE4-causing Munc18-1 mutants, fixed, and immunolabeled with anti–α-Syn antibody. Representative images of MKO-PC12 cells expressing EIEE4-causing Munc18-1 mutants and probed with endogenous α-Syn. Bar, 20 µm. Arrowheads indicate colocalized aggregates. (B) Percentage of colocalized aggregates per MKO-PC12 cell. (C) Percentage of MKO-PC12 cells containing aggregates. Data represent mean ± SEM. 10–20 cells were analyzed for each independent experiment (n = 3).

implies that the mutant-altered conformation can also be reached by the WT, although the aggregation of the latter is unlikely to be thermodynamically favored under normal conditions. Hence, our results suggest a high level of selectivity in the coaggregation (Kim et al., 2013; Martin et al., 2014).

Interestingly, EIEE4-causing mutant aggregates of Munc18-1 acted as seeds for Munc18-1^{WT} polymerization but were unable to trigger α-Syn aggregation in vitro, ruling out self-propagating activity of Munc18-1^{C180Y} polymers on α-Syn. Indeed, it would have been surprising to template the polymerization of a protein that is so structurally dissimilar. Our results also revealed that a high level of selectivity is required in the coaggregation, with known binders of Munc18-1 such as syntaxin1A (unpublished data) and SNAP25 excluded from the aggregates. Moreover, another protein with known aggregative properties, SOD1, did not coaggregate with Munc18-1 EIEE4-causing mutants, which strongly suggests some level of specificity for Munc18-1 binding to α-Syn.

Munc18-1 acts as a chaperone for α-Syn and controls its aggregative propensity

Munc18-1 human mutations are responsible for generating the strong epileptic phenotype observed in EIEE4 patients (Otsuka et al., 2010; Saitsu et al., 2010). Our data strongly suggest that the Munc18-1^{C180Y} mutation can cause protein misfolding, as well as a specific aggregation that recruits both endogenous Munc18-1 and α-Syn. This indicates a possible pathogenic gain of function. However, EIEE4-causing genetic alterations also include partial or full deletion of the Munc18-1 gene, suggesting that haploinsufficiency itself should be sufficient to promote an aggregative phenotype that leads to the pathology. Our results reveal that knocking out Munc18-1 in neurosecretory cells (MKO-PC12 cells) is sufficient to significantly increase the number of endogenous and expressed α-Syn aggregates, an effect that can be fully rescued by reexpression of Munc18-1^{WT} in these cells. This suggests that Munc18-1 plays a key role in chaperoning α-Syn and that Munc18-1 haploinsufficiency is sufficient to promote the aggregative phenotype.

A molecular chaperone is defined as a protein that controls the folding or unfolding and the assembly or disassembly of other proteins. One major function of chaperones is to prevent proteins and assembled protein complexes from aggregating (Kim et al., 2013; Saibil, 2013). The evidence provided by our study fits with this definition, as we demonstrate that Munc18-1 controls the aggregative propensity of α-Syn. We have found that EIEE-causing mutations of Munc18-1 coaggregate α-Syn both in vitro and when expressed in neurons and gene-edited neurosecretory cells. We also demonstrate that expression of these mutants can effectively recruit endogenous α-Syn into aggregates in neurons and gene-edited neurosecretory cells. Conversely, we have shown that expression of a PD-linked α-Syn mutant causes endogenous and expressed Munc18-1^{WT} to coaggregate with α-Syn. Finally, we have revealed that knocking out Munc18-1 increases the propensity of α-Syn to aggregate, a phenotype that can be fully rescued by Munc18-1 reexpression in a concentration-dependent manner. Together, these lines of evidence point to a critical role of Munc18-1 in preventing α-Syn aggregation and therefore fit with the definition of a chaperone. It is likely that Munc18-1 directly controls the aggregation of α-Syn, as we demonstrate that it directly binds to both endogenous and expressed α-Syn and that this binding is potentiated by EIEE4 mutations. Our findings therefore reveal that Munc18-1 is a molecular chaperone for α-Syn. This is not unexpected, as Munc18-1 is already known to chaperone

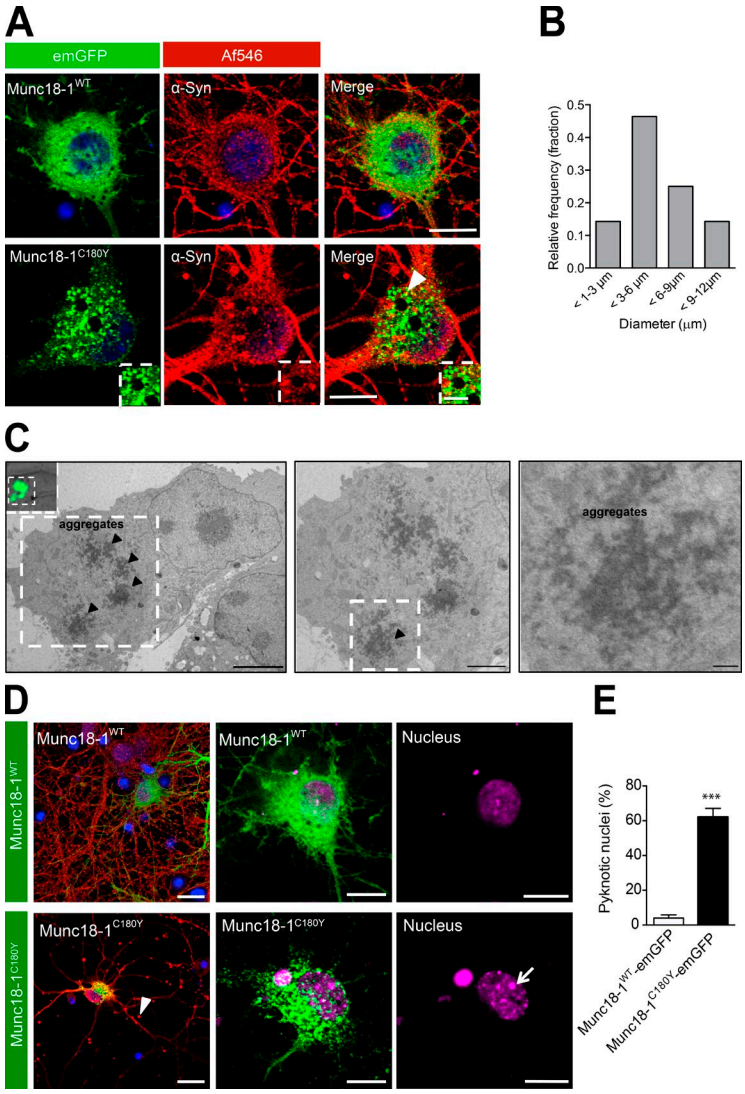

Figure 7. **Munc18-1^{C180Y} mutation recruits endogenous α-Syn aggregation and forms Lewy body–like structures.** Hippocampal neurons were transfected with Munc18-1^{WT}-emGFP and Munc18-1^{C180Y}-emGFP and immunolabeled with anti–α-Syn antibody. (A) Representative images of hippocampal neurons expressing Munc18-1C^{180Y} and probed for endogenous α-Syn. Bars: 20 µm; (magnified images) 5 µm. Arrowhead indicates colocalized aggregates. 11 neurons were analyzed per experiment (n = 3 independent experiment, so a total of 33 neurons were examined). (B) Relative frequency distribution of the size of Lewy body–like structures. (C) Representative correlative fluorescence electron micrograph of a Munc18-1^{C180Y}–positive aggregate in MKO-PC12 cells. Bars: (left) 5 µm; (center) 2 µm; (right) 500 nm. Arrowheads indicate cellular aggregates. (D) Representative images of hippocampal neurons transfected with either Munc18-1^{WT}-emGFP or Munc18-1^{C180Y}-emGFP. Nuclei were stained with DAPI. Bars, 10 µm. Arrowhead indicates a spheroid and arrow indicates pyknotic nucleus. (E) Percentage of pyknotic nuclei analyzed from Munc18-1^{WT}-emGFP (control) and Munc18-1^{C180Y}-emGFP transfected neurons. Data represent mean ± SEM (n = 6 regions of interest containing 7–12 transfected neurons each; ***, P < 0.001, unpaired Student's t test).

syntaxin1A (Pevsner et al., 1994; Misura et al., 2000; Malintan et al., 2009; Han et al., 2011), and the aggregative property of α-Syn can be reduced by the expression of molecular chaperones such as Hsp70 (Auluck et al., 2002; Maries et al., 2003; Cantuti-Castelvetri et al., 2005).

In summary, our results point to a critical role for Munc18-1 in reducing the formation of toxic α-Syn oligomers by chaperoning α-Syn, thereby controlling its aggregative propensity. Considering that α-Syn was recently shown to have a prion-like activity (Prusiner et al., 2015) and that Munc18-1 knockout mice show clear evidence of neurodegeneration (Law et al., 2016), uncovering the nature of the Munc18-1 binding site for α-Syn could have significant therapeutic value and potentially disease-modifying consequences for a number of neurodegenerative diseases, including PD, EIEE, and multiple system atrophy.

Materials and methods

Preparation of *Leishmania tarentolae* extract

L. tarentolae cell-free lysate was produced as described by previously (Mureev et al., 2009; Kovtun et al., 2011; Johnston and Alexandrov, 2014). In brief, *L. tarentolae* parrot strain was obtained as LEXSY host P10 from Jena Bioscience and cultured in TBGG medium containing 0.2% vol/vol penicillin/streptomycin (Thermo Fisher Scientific) and 0.05% wt/vol Hemin (MP Biomedicals). Cells were harvested by centrifugation at 2,500 *g*; washed twice by resuspension in 45 mM Hepes, pH 7.6, containing 250 mM sucrose, 100 mM potassium acetate, and 3 mM magnesium acetate; and resuspended to 0.25 g cells per gram suspension. Cells were placed in a cell disruption vessel (Parr Instruments) and incubated under 7,000-KPa nitrogen for 45 min, and then lysed by rapid release of pressure. The lysate was clarified by sequential centrifugation at 10,000 and 30,000 *g* and antisplice leader DNA leader oligonucleotide was added to 10 µM. The lysate was then desalted into 45 mM Hepes, pH 7.6, containing 100 mM potassium acetate and 3 mM magnesium acetate, supplemented with a coupled translation/transcription feeding solution, and then snap-frozen until required.

Gateway plasmids for cell-free protein expression

The proteins were cloned into the following cell-free expression Gateway destination vectors: N-terminal GFP tagged (pCellFree_G03), C-terminal sGFP tagged (pCellFree_G04), or C-terminal mCherry-cMyc tagged (pCellFree_G08; Gagoski et al., 2015). Transfer of ORFs between vectors was carried using Gateway PCR cloning protocol based on insert amplification with primers to attB1 and attB2 sites (forward primer: 5′-GGGGACAAGTTTGTACAAAAAAGCAGGCTT-3′ [nnn] 18–25; reverse primer: [nnnn] 5′-18-25AACCCAGCTTTCTTG TACAAAGTGGTCCCC-3′; Walhout et al., 2000).

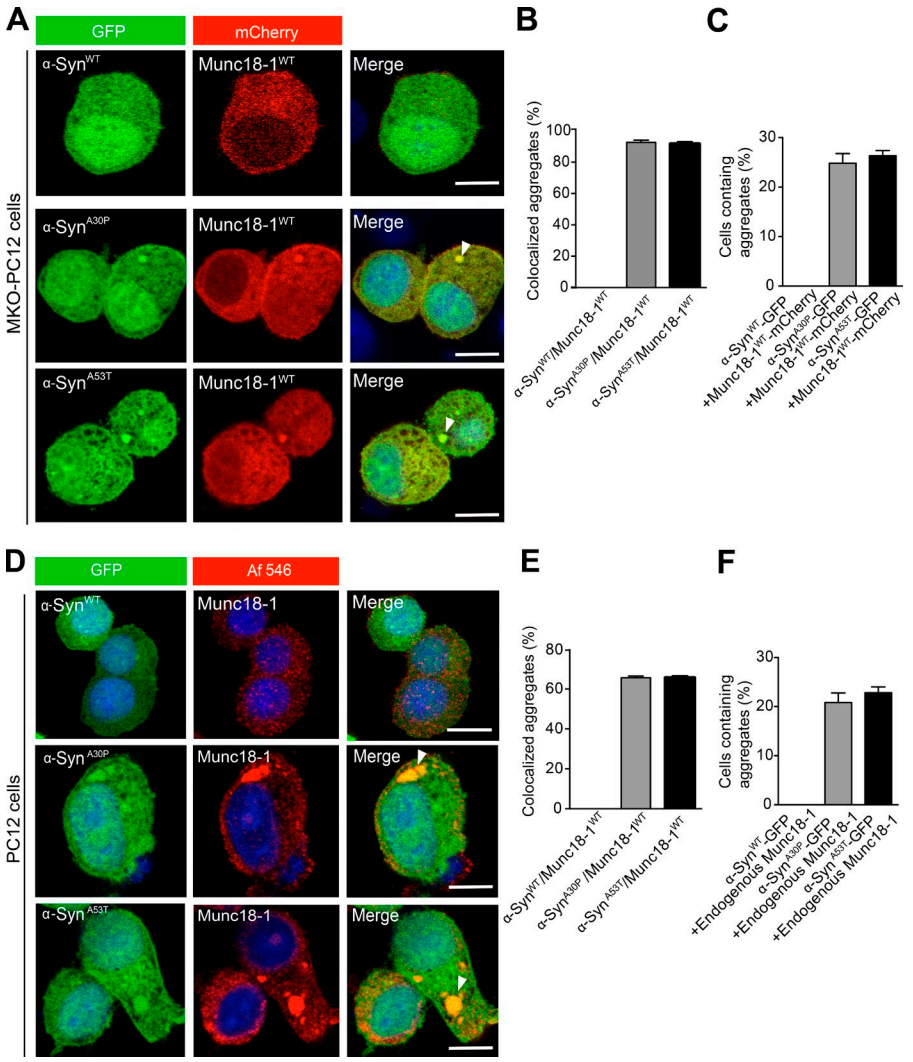

Figure 8. **PD-linked α-Syn mutants coaggregate Munc18-1^{WT} and endogenous Munc18-1.** (A) MKO-PC12 cells were cotransfected with either α-Syn^{WT}-GFP or indicated PD-linked α-Syn mutants and Munc18-1^{WT}-mCherry. Representative images showing coaggregates positive for PD-linked α-Syn mutants and Munc18-1^{WT}-mCherry in MKO-PC12 cells. Bars, 20 µm. (B) Percentage of colocalized aggregates. (C) Percentage of MKO-PC12 cells containing aggregates. 10–20 cells in each independent experiment were quantified. Data represent mean ± SEM; $n = 5$. (D) α-Syn^{WT}-GFP or PD-linked α-Syn mutants were transfected in PC12 cells and endogenous Munc18-1 was immunolabeled with anti–Munc18-1 antibody. Representative images showing coaggregates positive for GFP-tagged PD-linked α-Syn mutants and endogenous Munc18-1 in PC12 cells. Bars, 20 µm. Arrowheads indicate the colocalized aggregates. (E) Percentage of colocalized aggregates. (F) Percentage of PC12 cells containing aggregates. Data represent mean ± SEM. 10–20 cells were quantified in each independent experiment ($n = 3$).

Cell-free protein expression

Cell-free expression of proteins for interaction mapping used the eukaryotic *L. tarentolae* cell-free system. DNA templates for the various ORFs used the Gateway cloning system, with ribosome engagement with T7 transcribed mRNA mediated by the species-independent translation initiation site (Mureev et al., 2009). α-Syn was tagged with the genetically encoded fluorophores at the C terminus, as N terminus tagging prevents their natural oligomerization and aggregation. Coupled transcription/translation occurred for 3 h at 27°C unless otherwise described.

Single-molecule spectroscopy

Single-molecule spectroscopy was performed based on previous studies (Gambin et al., 2009, 2011; Martin et al., 2014). 20 µl of samples was used for each experiment and placed into a custom-made silicone 192-well plate equipped with a glass coverslip (ProSciTech Australia). Plates were analyzed on an LSM710 microscope (ZEISS) with a confocor3 module at room temperature. Two lasers (488 nm and 561 nm) were cofocused in solution using a 40× 1.2 NA water-immersion objective (ZEISS); fluorescence was collected and split into the GFP and mCherry channels by a 560-nm dichroic mirror. The GFP emission was further filtered by a 505- to 540-nm band-pass filter and the mCherry emission was filtered using a 580-nm long-pass filter.

The single-molecule multicolor detection method is based on a simple principle: the two excitation lasers are focused within the same point, creating a very small observation volume (~1 fl). The proteins are tagged with genetically encoded GFP and mCherry fluorophores. Proteins diffuse freely by Brownian motion, and they enter and exit the confocal volume constantly.

The mean intensity was calculated for both mCherry ($\langle I_c(t)\rangle$) and GFP traces ($\langle I_G(t)\rangle$). The time traces were acquired with 1-ms time "bins," and the large events were relatively rare, ensuring that the mean value correctly approximates the background of monomeric proteins.

The aggregates were detected as intense bursts of fluorescence, where the number of photons acquired in 1 ms were significantly higher than the mean value. We found that a "threshold" of 1,500 photons above the mean signal values efficiently separates the fluctuations of background and the high-amplitude bursts of the aggregates. Note that 1,500 photons correspond approximately to the simultaneous diffusion of 30–50 proteins.

For each time bin where $I_c(t) + I_G(t) > 1{,}500 + (\langle I_c(t)\rangle + \langle I_c(t)\rangle)$, the incorporation of GFP-tagged proteins into the mCherry-tagged aggregates was calculated as the ratio of mCherry signal to the total signal, after corrections of background:

$$C = \frac{\left(I_C(t) - \langle I_C(t)\rangle\right)}{\left(I_G(t) - \langle I_G(t)\rangle\right) + \left(I_C(t) - \langle I_C(t)\rangle\right)}.$$

The histograms of distribution of C values can be interpreted in terms of proportions of GFP and mCherry in the oligomers: a GFP-only

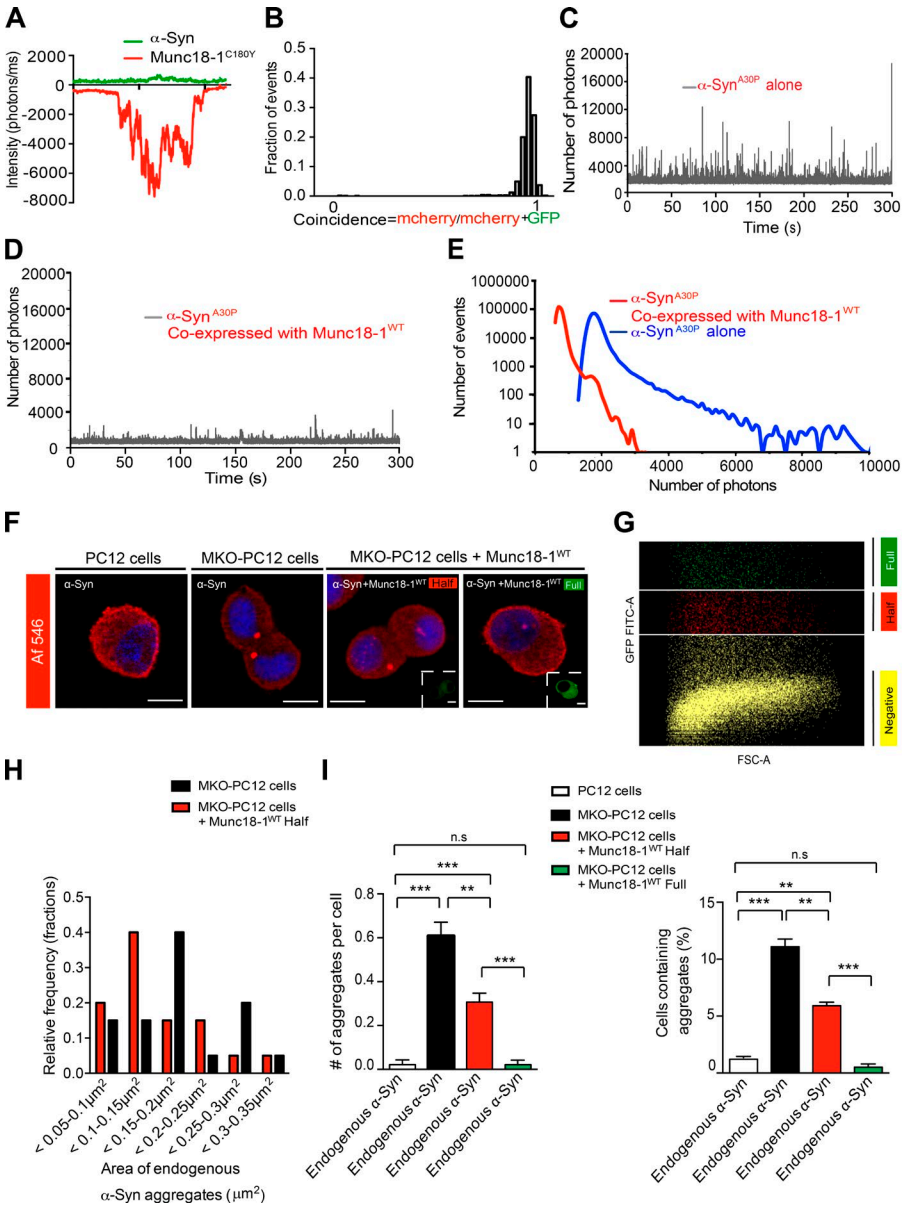

Figure 9. **Munc18-1 controls endogenous α-Syn propensity to aggregate in vitro and in gene-edited neurosecretory cells.** (A) Seeds of Munc18-1^{C180Y} do not recruit α-Syn in vitro. A single-molecule trace obtained from seed experiments. α-Syn-GFP is not recruited to the seeds of Munc18-1^{C180Y}-mCherry. (B) Histogram of single-molecule coincidence between α-Syn-GFP and seeds of Munc18-1^{C180Y}-mCherry. (C) A single-molecule trace obtained for cell-free lysates expressing α-Syn^{A30P}-GFP alone. (D) A single-molecule trace obtained for cell-free lysates coexpressing α-Syn^{A30P}-GFP and Munc18-1^{WT}-mCherry (E) Detailed analysis of the distribution of fluorescence bursts from C and D, showing a reduction in bright events caused by the chaperone activity of Munc18-1. (F) Munc18-1^{WT}-emGFP was transfected in MKO-PC12 cells, and FACS was applied to separate low-expressing from high-expressing Munc18-1 ^{WT}-emGFP transfected MKO-PC12 cells. MKO-PC12 cells together with control PC12 cells were platted for 4 h, fixed, and immunolabeled for α-Syn. Representative image of endogenous α-Syn from indicated cells. Bars, 20 µm. (G) FACS forward scatterplot showing gates used to select cells with half and full expression levels of Munc18-1^{WT}-emGFP (H) The area occupied by endogenous α-Syn was quantified and the frequency distribution plotted. (I) The number of aggregates per cell and the percentage of cells containing aggregates were measured in PC12 cells and Munc18-1^{WT}-emGFP low- to higher-expressing MKO-PC12 cells. Data represent mean ± SEM. 10–20 cells for each independent experiment were quantified (n = 3). One-way ANOVA was performed (**, P < 0.01; *** P < 0.001; n.s, not significant).

aggregate would appear at $C = 0$, whereas a mCherry-only burst would appear at $C = 1$. When the two fluorophores are codetected, the C values represent a direct measure of stoichiometry of incorporation in the mixed aggregate.

As shown by the examples of individual bursts traces, we can easily detect whether the large aggregate contains the two fluorophores. The histograms are shown as an overall quantification of all large events.

Antibodies and reagents

Mouse anti-Sx1a (S0644; clone HPC-1) and mouse anti–β-actin (A5316; clone AC-74) were obtained from Sigma-Aldrich, and anti–Munc18-1 (610336) was obtained from BD.

Mouse anti–α-Syn (27766) was obtained from Abcam. Mouse anti-VAMP2 (104211) was obtained from Synaptic Systems. PC12 cells and MKO-PC12 cells were maintained as described previously (Martin et al., 2013).

Munc18-1 single guide RNA (sgRNA) expression construct

A 20-bp guide sequence (5′-ATTGGCCTCAAGGCGGTGGT-3′) targeting DNA within the first exon of Munc18-1 was selected from an online CRISPR design tool. The sgRNA expression construction method has been described previously (Ran et al., 2013).

Transfection and cell sorting of MKO-PC12 cells

PC12 cells were cultured in six-well dishes to 70–80% confluence. Cells were transfected with 1 µg sequence-verified pSpCas9-Munc18-1 (sgRNA)-2A-GFP using Lipofectamine 2000 (Invitrogen). 48 h after transfection, cells were pelleted in DMEM and sorted in 96-well plates using a FACSAris II cell sorter (BD). Single cells from GFP-expressing cells (high expression population) were expanded to obtain individual clones.

Clone validation

Individual clones were lysed with 1% Triton X-100 and centrifuged at 14,000 rpm for 20 min at 4°C. The whole-cell lysates were eluted in 2× SDS sample buffer and analyzed by Western blot with specific antibody against Munc18-1. Genomic DNA was isolated from edited clones and nonedited PC12 cells (control). A region of exon1 of the Munc18-1 gene was amplified with genomic DNA specific primers (forward primer, 5′-CGGAGTCCGCGCGTCAGTCGGT-3′; reverse primer, 5′-ATAAAG

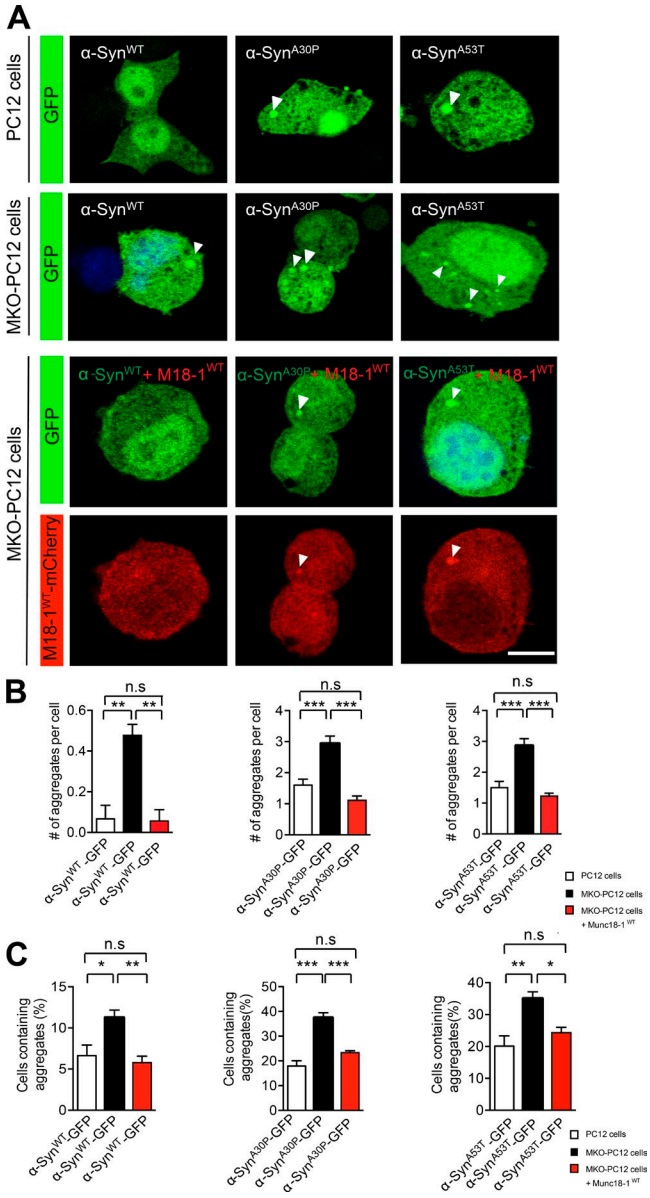

Figure 10. **Munc18-1^{WT} reexpression in MKO-PC12 cells rescues the propensity α-Syn^{WT} and two PD-linked α-Syn mutants to aggregate.** α-Syn^{WT}-GFP or PD-linked α-Syn mutants were transfected in PC12 cells or MKO-PC12 cells (top and middle). α-Syn^{WT}-GFP and Munc18-1^{WT}–mCherry or PD-linked α-Syn mutants and Munc18-1^{WT}-mCherry were cotransfected in MKO-PC12 cells to rescue the Munc18-1^{WT} expression (bottom). (A) Representative images of aggregates positive for α-Syn^{WT} and PD-linked α-Syn mutants in PC12 cells (top) or in MKO-PC12 cells (middle), and MKO-PC12 cells expressing Munc18-1^{WT}-mCherry (bottom). Bar, 20 µm. Arrowheads indicate the colocalized aggregates. The number of aggregates per cell (B) and the percentage of cells containing aggregates (C) were quantified. Data represent mean ± SEM. 10–20 cells for each independent experiment were quantified (n = 3; *, P < 0.05; **, P < 0.01; ***, P < 0.001; one way ANOVA).

GGGCGGATGGGGGAGGGA-3′). The PCR products were A-tailed and cloned into pGEM-T easy (Promega) and sequenced in the Australian Genome Research Facility, University of Queensland.

Cell transfection and neuronal culture

PC12 cells and MKO-PC12 cells were cotransfected with Munc18-1 and α-Syn constructs using Lipofectamine LTX (Invitrogen) according to the manufacturer's instruction and expressed 24–48 h before replating onto poly-D-lysine–coated glass-bottomed MatTek Corporation dishes or coverslips. Hippocampal rat neurons from E18 Sprague–Dawley rat pups were plated onto poly-L-lysine–coated dishes in Neurobasal growth medium supplemented with 2% B27 and 2 mM Glutamax. Neurons were switched to serum-free Neurobasal medium 24 h after seeding and medium was replaced twice per week. Transient transfection of hippocampal neurons was performed at 8–10 d in vitro using Lipofectamine 2000 (Invitrogen), and the cells were imaged 48 h after transfection. Approval for animal studies was obtained from the University of Queensland Animal Ethics Committee.

Immunofluorescence microscopy

PC12 cells and MKO-PC12 cells or hippocampal neurons were cotransfected with Munc18-1 and α-Syn constructs. Quantitative immunofluorescence was performed by collecting images with a 63× 1.40 NA oil-immersion objective on an LSM510 confocal microscope (ZEISS). The colocalization of aggregates was analyzed by a surface tool in Imaris (Bitplane). Munc18-1^{C180Y}-GFP aggregates were identified using a threshold background subtraction combining a minimum object size of 0.46 µm and minimum intensity of 19.2. We then compared the total number of Munc18-1^{C180Y} aggregates detected with the number of Munc18-1^{C180Y} aggregates that colocalized with α-Syn aggregates and expressed the result as percentage.

Immunoprecipitation and Western blotting

PC12 cells were transfected with the Munc18-1 constructs. The whole-cell lysates of Triton X-100 extracts were centrifuged at 14,000 rpm for 20 min at 4°C and cleared with protein A or G Sepharose overnight at 4°C, followed by four washes with ice-cold lysis buffer (1% Triton X-100, 1 mM EDTA, 1 mM EGTA, and complete EDTA-free protease inhibitor cocktails; Roche). Precleared lysates were then incubated with anti-GFP antibodies coupled to protein A or G Sepharose overnight at 4°C, followed by four washes with ice-cold lysis buffer and elution in 2× SDS sample buffer. The immunoprecipitated proteins were resolved by SDS-PAGE and probed by Western blot analysis with antibodies against Munc18-1, α-Syn, and β-actin.

NPY-hPLAP release assay

WT PC12 cells or MKO-PC12 cells were transfected with NPY-hPLAP plasmid and the indicated Munc18-1 for 48 h. Cells were washed and incubated with PSS buffer as a control (145 mM NaCl, 5.6 mM KCl, 0.5 mM $MgCl_2$, 5.6 mM glucose, and 15 mM Hepes-NaOH, pH 7.4) or stimulated with high K^+-PSS buffer (81 mM NaCl, 70 mM KCl, 2.2 mM $CaCl_2$, 0.5 mM $MgCl_2$, 5.6 mM glucose, and 15 mM Hepes-NaOH, pH 7.4) for 15 min at 37°C, and supernatants were collected. After collecting the supernatants, cells were lysed with 0.2% Triton X-100 to measure total NPY-hPLAP. The released and total NPY-hPLAP was measured using the chemiluminescent reporter gene assay system (Phospha-Light; Applied Biosystems) according to the manufacturer's instructions, and the results were expressed as a percentage of total NPY-hPLAP (Tomatis et al., 2013).

Statistical analyses

All experiments were repeated at least three times. Data analysis was performed using unpaired, Student's *t* tests or one-way analysis of variance (ANOVA) followed by multiple comparisons test as stated in the figures. Data were considered significant at $P < 0.05$. Values are expressed as means ± SEM, and the level of significance is designated in the figure legend as follows: *, $P < 0.05$; **, $P < 0.01$; ***, $P < 0.001$.

Online supplemental material

Fig. S1 shows functional validation of MKO-PC12 cells and rescue of Munc18-1 expression levels. Fig. S2 shows the Munc18-1C180Y mutant coaggregates with Munc18-1WT in MKO-PC12 cells and hippocampal neurons. Fig. S3 shows Munc18-1C180Y mutants cause Lewy body–like structures positive for Munc18-1WT and α-Syn. Fig. S4 shows PD-linked α-Syn mutants form Mun18-1WT and endogenous Munc18-1-positive Lewy body–like structures. Fig. S5 shows endogenous Munc18-1 interacts with endogenous α-Syn in cortical neurons and PC12 cells. Online supplemental material is available at http://www.jcb.org/cgi/content/full/jcb.201512016/DC1. Additional data are available in the JCB DataViewer at http://dx.doi.org/10.1083/jcb.201512016.dv.

Acknowledgments

We thank Andreas Papadopulos, Sally Martin, Kirill Alexandrov, and Rowan Tweedale for help and critical appraisal of the manuscript. We also thank Matthijs Verhage for insightful discussion at an early stage of this study. Electron microscopy was performed in the Australian Microscopy and Microanalysis Facility at the Centre for Microscopy and Microanalysis at the University of Queensland. Imaging work was performed in the Queensland Brain Institute's Advanced Microscopy Facility. Flow cytometry was performed by Virginia Nink and Geoff Osborne at the Queensland Brain Institute's Flow Cytometry Facility.

This research was supported by a project grant from the National Health and Medical Research Council of Australia to F.A. Meunier (GNT1044014GNT). B.M. Collins is a National Health and Medical Research Council Career Development Fellow (GNT1061574GNT), and F.A. Meunier is a National Health and Medical Research Council Senior Research Fellow (GNT1060075). Y.J. Chai holds an Australian Postgraduate Award and a Queensland Brain Institute Top-Up Scholarship.

The authors declare no competing financial interests.

Author contributions: Y.J. Chai conducted the experiments and was involved in the experimental design (Fig. 2; Fig. 3, B–D; Fig. 5; Fig. 6; Fig. 7, A, B, D, and E; Fig. 8; Fig. 9, F–I; Fig. 10; Fig. S1, A and D; and Figs. S2–S5). E. Sierecki and Y. Gambin performed the work shown in Figs. 1 (B–I), 4, and 9 (A–E) under the supervision of R.G. Parton. V.M. Tomatis and R.S. Gormal performed the work shown in Fig. S1 (B and C). I.C. Morrow performed the work shown in Fig. 7 C. B.M. Collins performed the work shown in Figs. 1 A and 3 A. D. Xia contributed new reagents for CRISPR cells in Fig. S1 A under the supervision of J. Götz. N. Gils contributed new reagents in single-molecule fluorescence experiments. F.A. Meunier and Y. Gambin supervised the study. All authors contributed to writing of the manuscript.

Submitted: 4 December 2015
Accepted: 3 August 2016

References

Alvarez-Barón, E., C.G. Bien, J. Schramm, C.E. Elger, A.J. Becker, and S. Schoch. 2008. Autoantibodies to Munc18, cerebral plasma cells and B-lymphocytes in Rasmussen encephalitis. *Epilepsy Res.* 80:93–97. http://dx.doi.org/10.1016/j.eplepsyres.2008.03.007

Auluck, P.K., H.Y. Chan, J.Q. Trojanowski, V.M. Lee, and N.M. Bonini. 2002. Chaperone suppression of α-synuclein toxicity in a *Drosophila* model for Parkinson's disease. *Science.* 295:865–868. http://dx.doi.org/10.1126/science.1067389

Barcia, G., N. Chemaly, S. Gobin, M. Milh, P. Van Bogaert, C. Barnerias, A. Kaminska, O. Dulac, I. Desguerre, V. Cormier, et al. 2014. Early epileptic encephalopathies associated with STXBP1 mutations: could we better delineate the phenotype? *Eur. J. Med. Genet.* 57:15–20. http://dx.doi.org/10.1016/j.ejmg.2013.10.006

Burré, J., M. Sharma, and T.C. Südhof. 2014. α-Synuclein assembles into higher-order multimers upon membrane binding to promote SNARE complex formation. *Proc. Natl. Acad. Sci. USA.* 111:E4274–E4283. http://dx.doi.org/10.1073/pnas.1416598111

Cantuti-Castelvetri, I., J. Klucken, M. Ingelsson, K. Ramasamy, P.J. McLean, M.P. Frosch, B.T. Hyman, and D.G. Standaert. 2005. Alpha-synuclein and chaperones in dementia with Lewy bodies. *J. Neuropathol. Exp. Neurol.* 64:1058–1066. http://dx.doi.org/10.1097/01.jnen.0000190063.90440.69

Deprez, L., S. Weckhuysen, P. Holmgren, A. Suls, T. Van Dyck, D. Goossens, J. Del-Favero, A. Jansen, K. Verhaert, L. Lagae, et al. 2010. Clinical spectrum of early-onset epileptic encephalopathies associated with STX BP1 mutations. *Neurology.* 75:1159–1165. http://dx.doi.org/10.1212/WNL.0b013e3181f4d7bf

Donovan, L.E., L. Higginbotham, E.B. Dammer, M. Gearing, H.D. Rees, Q. Xia, D.M. Duong, N.T. Seyfried, J.J. Lah, and A.I. Levey. 2012. Analysis of a membrane-enriched proteome from postmortem human brain tissue in Alzheimer's disease. *Proteomics Clin. Appl.* 6:201–211. http://dx.doi.org/10.1002/prca.201100068

Gagoski, D., S. Mureev, N. Giles, W. Johnston, M. Dahmer-Heath, D. Škalamera, T.J. Gonda, and K. Alexandrov. 2015. Gateway-compatible vectors for high-throughput protein expression in pro- and eukaryotic cell-free systems. *J. Biotechnol.* 195:1–7. http://dx.doi.org/10.1016/j.jbiotec.2014.12.006

Galvin, J.E., K. Uryu, V.M. Lee, and J.Q. Trojanowski. 1999. Axon pathology in Parkinson's disease and Lewy body dementia hippocampus contains alpha-, beta-, and gamma-synuclein. *Proc. Natl. Acad. Sci. USA.* 96:13450–13455. http://dx.doi.org/10.1073/pnas.96.23.13450

Gambin, Y., A. Schug, E.A. Lemke, J.J. Lavinder, A.C. Ferreon, T.J. Magliery, J.N. Onuchic, and A.A. Deniz. 2009. Direct single-molecule observation of a protein living in two opposed native structures. *Proc. Natl. Acad. Sci. USA.* 106:10153–10158. http://dx.doi.org/10.1073/pnas.0904461106

Gambin, Y., V. VanDelinder, A.C. Ferreon, E.A. Lemke, A. Groisman, and A.A. Deniz. 2011. Visualizing a one-way protein encounter complex by ultrafast single-molecule mixing. *Nat. Methods.* 8:239–241. http://dx.doi.org/10.1038/nmeth.1568

Hamdan, F.F., A. Piton, J. Gauthier, A. Lortie, F. Dubeau, S. Dobrzeniecka, D. Spiegelman, A. Noreau, S. Pellerin, M. Côté, et al. 2009. De novo STX BP1 mutations in mental retardation and nonsyndromic epilepsy. *Ann. Neurol.* 65:748–753. http://dx.doi.org/10.1002/ana.21625

Hamdan, F.F., J. Gauthier, S. Dobrzeniecka, A. Lortie, L. Mottron, M. Vanasse, G. D'Anjou, J.C. Lacaille, G.A. Rouleau, and J.L. Michaud. 2011. Intellectual disability without epilepsy associated with STXBP1 disruption. *Eur. J. Hum. Genet.* 19:607–609. http://dx.doi.org/10.1038/ejhg.2010.183

Han, G.A., N.T. Malintan, N.M. Saw, L. Li, L. Han, F.A. Meunier, B.M. Collins, and S. Sugita. 2011. Munc18-1 domain-1 controls vesicle docking and secretion by interacting with syntaxin-1 and chaperoning it to the plasma membrane. *Mol. Biol. Cell.* 22:4134–4149. http://dx.doi.org/10.1091/mbc.E11-02-0135

Han, L., T. Jiang, G.A. Han, N.T. Malintan, L. Xie, L. Wang, F.W. Tse, H.Y. Gaisano, B.M. Collins, F.A. Meunier, and S. Sugita. 2009. Rescue of Munc18-1 and -2 double knockdown reveals the essential functions of interaction between Munc18 and closed syntaxin in PC12 cells. *Mol. Biol. Cell.* 20:4962–4975. http://dx.doi.org/10.1091/mbc.E09-08-0712

Jacobs, E.H., R.J. Williams, and P.T. Francis. 2006. Cyclin-dependent kinase 5, Munc18a and Munc18-interacting protein 1/X11alpha protein up-regulation in Alzheimer's disease. *Neuroscience.* 138:511–522. http://dx.doi.org/10.1016/j.neuroscience.2005.11.017

Johnston, W.A., and K. Alexandrov. 2014. Production of eukaryotic cell-free lysate from *Leishmania tarentolae*. *Methods Mol. Biol.* 1118:1–15. http://dx.doi.org/10.1007/978-1-62703-782-2_1

Kim, Y.E., M.S. Hipp, A. Bracher, M. Hayer-Hartl, and F.U. Hartl. 2013. Molecular chaperone functions in protein folding and proteostasis. *Annu.*

Rev. Biochem. 82:323–355. http://dx.doi.org/10.1146/annurev-biochem-060208-092442

Kovtun, O., S. Mureev, W. Jung, M.H. Kubala, W. Johnston, and K. Alexandrov. 2011. *Leishmania* cell-free protein expression system. *Methods.* 55:58–64. http://dx.doi.org/10.1016/j.ymeth.2011.06.006

Lang, L., P. Zetterström, T. Brännström, S.L. Marklund, J. Danielsson, and M. Oliveberg. 2015. SOD1 aggregation in ALS mice shows simplistic test tube behavior. *Proc. Natl. Acad. Sci. USA.* 112:9878–9883. http://dx.doi.org/10.1073/pnas.1503328112

Law, C., M. Schaan Profes, M. Levesque, J.A. Kaltschmidt, M. Verhage, and A. Kania. 2016. Normal molecular specification and neurodegenerative disease-like death of spinal neurons lacking the SNARE-associated synaptic protein Munc18-1. *J. Neurosci.* 36:561–576. http://dx.doi.org/10.1523/JNEUROSCI.1964-15.2016

Malintan, N.T., T.H. Nguyen, L. Han, C.F. Latham, S.L. Osborne, P.J. Wen, S.J. Lim, S. Sugita, B.M. Collins, and F.A. Meunier. 2009. Abrogating Munc18-1-SNARE complex interaction has limited impact on exocytosis in PC12 cells. *J. Biol. Chem.* 284:21637–21646. http://dx.doi.org/10.1074/jbc.M109.013508

Maries, E., B. Dass, T.J. Collier, J.H. Kordower, and K. Steece-Collier. 2003. The role of alpha-synuclein in Parkinson's disease: insights from animal models. *Nat. Rev. Neurosci.* 4:727–738. http://dx.doi.org/10.1038/nrn1199

Martin, S., V.M. Tomatis, A. Papadopulos, M.P. Christie, N.T. Malintan, R.S. Gormal, S. Sugita, J.L. Martin, B.M. Collins, and F.A. Meunier. 2013. The Munc18-1 domain 3a loop is essential for neuroexocytosis but not for syntaxin-1A transport to the plasma membrane. *J. Cell Sci.* 126:2353–2360. http://dx.doi.org/10.1242/jcs.126813

Martin, S., A. Papadopulos, V.M. Tomatis, E. Sierecki, N.T. Malintan, R.S. Gormal, N. Giles, W.A. Johnston, K. Alexandrov, Y. Gambin, et al. 2014. Increased polyubiquitination and proteasomal degradation of a Munc18-1 disease-linked mutant causes temperature-sensitive defect in exocytosis. *Cell Reports.* 9:206–218. http://dx.doi.org/10.1016/j.celrep.2014.08.059

McKeith, I. 2004. Dementia with Lewy bodies. *Dialogues Clin. Neurosci.* 6:333–341.

Mignot, C., M.L. Moutard, O. Trouillard, I. Gourfinkel-An, A. Jacquette, B. Arveiler, F. Morice-Picard, D. Lacombe, C. Chiron, D. Ville, et al. 2011. STXBP1-related encephalopathy presenting as infantile spasms and generalized tremor in three patients. *Epilepsia.* 52:1820–1827. http://dx.doi.org/10.1111/j.1528-1167.2011.03163.x

Misura, K.M., R.H. Scheller, and W.I. Weis. 2000. Three-dimensional structure of the neuronal-Sec1-syntaxin 1a complex. *Nature.* 404:355–362. http://dx.doi.org/10.1038/35006120

Mureev, S., O. Kovtun, U.T. Nguyen, and K. Alexandrov. 2009. Species-independent translational leaders facilitate cell-free expression. *Nat. Biotechnol.* 27:747–752. http://dx.doi.org/10.1038/nbt.1556

Orimo, S., T. Uchihara, A. Nakamura, F. Mori, A. Kakita, K. Wakabayashi, and H. Takahashi. 2008. Axonal α-synuclein aggregates herald centripetal degeneration of cardiac sympathetic nerve in Parkinson's disease. *Brain.* 131:642–650. http://dx.doi.org/10.1093/brain/awm302

Otsuka, M., H. Oguni, J.S. Liang, H. Ikeda, K. Imai, K. Hirasawa, K. Imai, E. Tachikawa, K. Shimojima, M. Osawa, and T. Yamamoto. 2010. STXBP1 mutations cause not only Ohtahara syndrome but also West syndrome--result of Japanese cohort study. *Epilepsia.* 51:2449–2452. http://dx.doi.org/10.1111/j.1528-1167.2010.02767.x

Papadopulos, A., S. Martin, V.M. Tomatis, R.S. Gormal, and F.A. Meunier. 2013. Secretagogue stimulation of neurosecretory cells elicits filopodial extensions uncovering new functional release sites. *J. Neurosci.* 33:19143–19153. http://dx.doi.org/10.1523/JNEUROSCI.2634-13.2013

Pevsner, J., S.C. Hsu, and R.H. Scheller. 1994. n-Sec1: a neural-specific syntaxin-binding protein. *Proc. Natl. Acad. Sci. USA.* 91:1445–1449. http://dx.doi.org/10.1073/pnas.91.4.1445

Polymeropoulos, M.H., C. Lavedan, E. Leroy, S.E. Ide, A. Dehejia, A. Dutra, B. Pike, H. Root, J. Rubenstein, R. Boyer, et al. 1997. Mutation in the alpha-synuclein gene identified in families with Parkinson's disease. *Science.* 276:2045–2047. http://dx.doi.org/10.1126/science.276.5321.2045

Prusiner, S.B., A.L. Woerman, D.A. Mordes, J.C. Watts, R. Rampersaud, D.B. Berry, S. Patel, A. Oehler, J.K. Lowe, S.N. Kravitz, et al. 2015. Evidence for α-synuclein prions causing multiple system atrophy in humans with parkinsonism. *Proc. Natl. Acad. Sci. USA.* 112:E5308–E5317. http://dx.doi.org/10.1073/pnas.1514475112

Ran, F.A., P.D. Hsu, J. Wright, V. Agarwala, D.A. Scott, and F. Zhang. 2013. Genome engineering using the CRISPR-Cas9 system. *Nat. Protoc.* 8:2281–2308. http://dx.doi.org/10.1038/nprot.2013.143

Saibil, H. 2013. Chaperone machines for protein folding, unfolding and disaggregation. *Nat. Rev. Mol. Cell Biol.* 14:630–642. http://dx.doi.org/10.1038/nrm3658

Saitsu, H., M. Kato, T. Mizuguchi, K. Hamada, H. Osaka, J. Tohyama, K. Uruno, S. Kumada, K. Nishiyama, A. Nishimura, et al. 2008. De novo mutations in the gene encoding STXBP1 (MUNC18-1) cause early infantile epileptic encephalopathy. *Nat. Genet.* 40:782–788. http://dx.doi.org/10.1038/ng.150

Saitsu, H., M. Kato, I. Okada, K.E. Orii, T. Higuchi, H. Hoshino, M. Kubota, H. Arai, T. Tagawa, S. Kimura, et al. 2010. STXBP1 mutations in early infantile epileptic encephalopathy with suppression-burst pattern. *Epilepsia.* 51:2397–2405. http://dx.doi.org/10.1111/j.1528-1167.2010.02728.x

Spillantini, M.G., M.L. Schmidt, V.M. Lee, J.Q. Trojanowski, R. Jakes, and M. Goedert. 1997. α-synuclein in Lewy bodies. *Nature.* 388:839–840. http://dx.doi.org/10.1038/42166

Tavyev Asher, Y.J., and F. Scaglia. 2012. Molecular bases and clinical spectrum of early infantile epileptic encephalopathies. *Eur. J. Med. Genet.* 55:299–306. http://dx.doi.org/10.1016/j.ejmg.2012.04.002

Tomatis, V.M., A. Papadopulos, N.T. Malintan, S. Martin, T. Wallis, R.S. Gormal, J. Kendrick-Jones, F. Buss, and F.A. Meunier. 2013. Myosin VI small insert isoform maintains exocytosis by tethering secretory granules to the cortical actin. *J. Cell Biol.* 200:301–320. http://dx.doi.org/10.1083/jcb.201204092

Verhage, M., A.S. Maia, J.J. Plomp, A.B. Brussaard, J.H. Heeroma, H. Vermeer, R.F. Toonen, R.E. Hammer, T.K. van den Berg, M. Missler, et al. 2000. Synaptic assembly of the brain in the absence of neurotransmitter secretion. *Science.* 287:864–869. http://dx.doi.org/10.1126/science.287.5454.864

Walhout, A.J.M., G.F. Temple, M.A. Brasch, J.L. Hartley, M.A. Lorson, S. van den Heuvel, and M. Vidal. 2000. GATEWAY recombinational cloning: application to the cloning of large numbers of open reading frames or ORFeomes. *Methods Enzymol.* 328:575–592. http://dx.doi.org/10.1016/S0076-6879(00)28419-X

Wang, J., G.W. Farr, D.H. Hall, F. Li, K. Furtak, L. Dreier, and A.L. Horwich. 2009. An ALS-linked mutant SOD1 produces a locomotor defect associated with aggregation and synaptic dysfunction when expressed in neurons of *Caenorhabditis elegans*. *PLoS Genet.* 5:e1000350. http://dx.doi.org/10.1371/journal.pgen.1000350